

FUV IRRADIATED DISK ATMOSPHERES: LY α AND THE ORIGIN OF HOT H₂ EMISSION

MÁTÉ ÁDÁMKOVICS¹, JOAN R. NAJITA², AND ALFRED E. GLASSGOLD¹

¹Astronomy Department, 501 Campbell Hall, University of California, Berkeley, CA 94720
mate@berkeley.edu and aglassgold@berkeley.edu

²National Optical Astronomical Observatory, 950 North Cherry Avenue, Tucson, AZ 85719; najita@noao.edu

Draft version September 21, 2017

ABSTRACT

Protoplanetary disks are strongly irradiated by a stellar FUV spectrum that is dominated by Ly α photons. We investigate the impact of stellar Ly α irradiation on the terrestrial planet region of disks ($\lesssim 1$ AU) using an updated thermal-chemical model of a disk atmosphere irradiated by stellar FUV and X-rays. The radiative transfer of Ly α is implemented in a simple approach that includes scattering by H I and absorption by molecules and dust. Because of their non-radial propagation path, scattered Ly α photons deposit their energy deeper in the disk atmosphere than the radially propagating FUV continuum photons. We find that Ly α has a significant impact on the thermal structure of the atmosphere. Photochemical heating produced by scattered Ly α photons interacting with water vapor and OH leads to a layer of hot (1500 – 2500 K) molecular gas. The temperature in the layer is high enough to thermally excite the H₂ to vibrational levels from which they can be fluoresced by Ly α to produce UV fluorescent H₂ emission. The resulting atmospheric structure may help explain the origin of UV fluorescent H₂ that is commonly observed from classical T Tauri stars.

Subject headings: planetary systems: protoplanetary disks — radiation mechanisms: thermal — astrochemistry

1. INTRODUCTION

Stellar FUV irradiation is expected to strongly affect the properties of protoplanetary disk atmospheres (e.g., Aikawa & Herbst 1999; Willacy & Langer 2000; Markwick et al. 2002; van Zadelhoff et al. 2003; Gorti & Hollenbach 2004, 2008; Kamp & Dullemond 2004; Jonkheid et al. 2004; Nomura et al. 2007; Agúndez et al. 2008; Bethell & Bergin 2009; Ercolano et al. 2009; Woitke et al. 2009; Woods & Willacy 2009; Heinzeller et al. 2011; Bethell & Bergin 2011; Fogel et al. 2011; Cleeves et al. 2011; Walsh et al. 2012; Akimkin et al. 2013; Du & Bergin 2014). FUV photons (912 – 2000 Å) not only ionize atoms, dissociate molecules, and contribute to photoelectric heating, but they also induce photochemical heating (Bethell & Bergin 2009; Glassgold et al. 2009; Woitke et al. 2009; Gorti et al. 2011; Ádámkovics et al. 2014; Glassgold & Najita 2015). The absorption of FUV photons in disk atmospheres can shield the disk midplane from irradiation (Bethell & Bergin 2009; Glassgold et al. 2009; Ádámkovics et al. 2014).

The stellar FUV radiation field has contributions from both the continuum and Ly α . Valuable clues to the strength of the Ly α component are provided by observations of UV fluorescent H₂ emission from T Tauri stars (TTS). The emission, which is well explained by strong dipole electronic transitions pumped for the most part by Ly α photons from excited vibrational levels of H₂ (Ardila et al. 2002; Herczeg et al. 2002), is detected commonly from the inner regions of protoplanetary disks. In the *Hubble Space Telescope (HST)* Cosmic Origins Spectrograph (COS) survey reported by France et al. (2012), fluorescent H₂ emission is detected from all accreting young stars (classical T Tauri stars; CTTS). Spectrally

resolved line profiles of the H₂ emission are consistent with the bulk of the emission arising from a circumstellar disk at radii within an AU (France et al. 2012). If the H₂ absorption lines are optically thin, the observed H₂ fluorescent emission can be used to reconstruct the Ly α luminosity incident on the disk. Studies that have used this approach find that Ly α is the dominant component ($\sim 80\%$) of the stellar FUV field (e.g., Herczeg et al. 2004; Schindhelm et al. 2012).

A TTS FUV field that is dominated by Ly α may impact the disk chemistry significantly (Bergin et al. 2003). Several recent studies have included stellar Ly α as a distinct component of the stellar FUV field. Bethell & Bergin (2011) have explored in detail the effect of H I resonant scattering on Ly α transport in TTS disks that have experienced significant dust settling. Models that include photodissociation by Ly α separately from the FUV continuum can bring model abundance ratios into better agreement with observations of outer disks (Fogel et al. 2011; Walsh et al. 2012). Detailed and sophisticated models have also explored the effect of Ly α on the water vapor distribution in disks (Du & Bergin 2014).

Ly α may affect disk properties significantly not only because it is more luminous, but also because of the different path that Ly α photons take in reaching the disk. As described by Bethell & Bergin (2011, hereafter BB11), stellar Ly α photons are strongly scattered by H I in the upper disk atmosphere. Photons scattered downward take a much more direct path into the disk than stellar continuum photons, which propagate through the disk at an oblique angle. The latter traverse a column of material along the line of sight from the star to a given depth into the disk that is much larger than the vertical column, and are likely to be strongly absorbed higher in the atmosphere. As a result, Ly α is expected to dominate

the UV photon field at large vertical column densities.

Despite the significance of these inferences from UV fluorescent H₂ emission, the origin of the disk conditions that produce the UV H₂ emission have been difficult to explain. Populating the excited vibrational levels of H₂ that can couple to the Ly α field requires a gas temperature that is unusually high for molecular gas (~ 2500 K) if the excitation is thermal (Herczeg et al. 2004; Schindhelm et al. 2012). Since these temperatures are larger than have been expected for H₂ in protoplanetary disk atmospheres (e.g., Woitke et al. 2009; Walsh et al. 2012; Glassgold et al. 2004), it is often assumed that the emitting H₂ is populated nonthermally, by UV and X-ray emission, as in the model of Nomura et al. (2007). However, if there is a mechanism for heating the molecular gas to ~ 2500 K, then the excited vibrational levels of H₂ can be populated thermally.

Here we revisit the problem of the origin of hot H₂ emission from disks using an expanded thermal-chemical model of protoplanetary disk atmospheres that explores the role of Ly α in heating the atmosphere. The earlier version of our model implemented irradiation by stellar FUV continuum photons and a preliminary treatment of photochemical heating by H₂O and OH (Ádámkóvics et al. 2014, hereafter AGN14). In the present study, we include irradiation by stellar Ly α , self-shielding in the 900–1000 Å band, and an improved implementation of photochemical heating. The Ly α radiative transfer is treated in a schematic way.

We find that Ly α irradiation is an important heat source for disk atmospheres. Our model can account for the characteristic properties of the hot H₂: its characteristic temperature, column density, and emitting radii. Our model and the updates to it are described in Section 2. In Section 3 we demonstrate the role of Ly α heating in determining the thermal and chemical structure of the atmosphere. These results are discussed in Section 4 and we summarize our findings in Section 5.

2. THERMAL-CHEMICAL MODEL

We use a thermal-chemical model of an X-ray and FUV irradiated disk that was most recently described in AGN14. The model builds on the work presented in Glassgold et al. (2004), Glassgold et al. (2009) and Ádámkóvics et al. (2011). As described in our previous work, the disk model atmosphere has a layered structure, with a hot (~ 5000 K) atomic layer overlying warm (~ 800 K) molecular and cool (~ 500 K) molecular layers. The resulting properties of the model atmosphere, such as warm columns of species and their radial extent, are in good agreement with the general molecular emission properties of *Spitzer* spectra of protoplanetary disks (Najita et al. 2011, AGN14).

The model adopts a static disk density and dust temperature structure from D’Alessio et al. (1999), with stellar and disk parameters listed in Table 1. As in AGN14, we assume dust properties (Table 1) that take into account that large grains settle to the midplane and leave a reduced population of small grains in the atmosphere. The grain size parameter a_g corresponds to a decrease in grain surface area by a factor of 20 compared to interstellar conditions, and a dust surface area per hydrogen nucleus that is $S_d \approx 8 \times 10^{-23}$ cm². A set of thermal

Table 1
Reference Model Parameters

Parameter	Symbol	Value
Stellar mass	M_*	$0.5 M_\odot$
Stellar radius	R_*	$2 R_\odot$
Stellar temperature	T_*	4000 K
Disk mass	M_D	$0.005 M_\odot$
Disk accretion rate	\dot{M}	$10^{-8} M_\odot \text{ yr}^{-1}$
Dust to gas ratio	ρ_d/ρ_g	0.01
Dust grain size	a_g	$0.7 \mu\text{m}$
Dust extinction	Q_{ext}	1.0
X-ray temperature	T_X	1 keV
X-ray luminosity	L_X	$2 \times 10^{30} \text{ erg s}^{-1}$
FUV continuum luminosity ^a	L_{FUV}	$1 \times 10^{31} \text{ erg s}^{-1}$
Ly α /FUV continuum ^b	η	3
Accretion heating	α_h	0.5

^a The FUV continuum luminosity is integrated from 1100–2000 Å and excludes Ly α , so that it is smaller than the value used in AGN14.

^b The ratio of the unattenuated downward Ly α photon number flux to the radially-propagating FUV continuum number flux in 1200–1700 Å band.

and chemical rate equations is used to determine the gas temperature and species abundances. The primary improvements to the model are in the treatment of FUV radiation and a more complete set of photodissociation pathways that use the stellar FUV field to heat the gas. Whereas we had previously included the photodissociation of water and OH (AGN14), here we also include the FUV photochemistry of additional abundant molecules and atoms and adopt the photochemical heating rates detailed in Glassgold & Najita (2015, hereafter GN15). Most notably, we now consider the radiative transfer and photochemistry of Ly α as separate from the FUV continuum.

In order to explore the effect of Ly α radiation on the disk atmosphere, we adopt a schematic treatment of its radiative transfer (scattering and absorption) that is based on detailed work in the literature, as described below. Scattering of FUV continuum photons (mostly forward) by grains is not considered. While we find that the propagation path of Ly α has a significant impact on the properties of the atmosphere (Section 3), our assumptions suggest that these results should be considered illustrative rather than quantitative. An improved FUV radiative transfer that includes scattering effects in a more realistic way is needed to understand the effect of Ly α on the detailed properties of the atmosphere.

The model presented here suffers from some additional shortcomings. Gas pressure balance is not enforced in that our calculation of the gas temperature does not alter the density structure of the atmosphere, as in the D’Alessio et al. (1999) model. We effectively assume that dust heating dominates in determining the density structure of the atmosphere. Because the gas temperature exceeds that of the dust in the atmosphere, we therefore tend to overestimate the density. We further assume that the dust abundance and size distribution are the same at all heights and radii in the atmosphere. Transport of material (radial or vertical) is also not considered, and we assume that the chemical timescales are rapid enough that abundances and thermal rates are determined by local conditions.

These effects are also likely to be more prominent at

smaller disk radii. This is particularly relevant as the dust is important for attenuating the FUV, for H₂ formation, and for thermal accommodation of the gas at high densities. Detailed consideration of changes in the dust profile with height, radius, and time are all very interesting and will be the subject of future work. In particular, at radii within ~ 0.1 AU the dust structure of the inner rim may be important for determining the radiation environment in the terrestrial planet region. For now, however, we describe a simplified treatment below.

2.1. FUV Radiative Transfer and Photochemistry

Previous work in the literature serves as a valuable guide to understanding the propagation of Ly α in disk atmospheres. Studies have found that Ly α emitted by the star can be scattered by intervening H I, e.g., in a wind, before it reaches the disk (Herczeg et al. 2004; Schindhelm et al. 2012). H I in the atomic layer at the disk surface will also scatter arriving Ly α photons so that they emerge roughly perpendicular to the disk surface (BB11). While a large fraction of the stellar Ly α photons may, in this way, be scattered away (reflected) from the disk, the fraction that passes through the atomic layer travels a path more directly downward into the disk, in contrast to the FUV continuum photons, which propagate at an oblique angle into the disk.

Quantitative results obtained in the earlier studies suggest a simple way to implement Ly α irradiation in our model. In their detailed Monte Carlo calculation of how Ly α photons interact with the gaseous disk, BB11 start out with a number flux of Ly α photons 6 times larger than the FUV continuum flux at the star. Upon leaving the star, Ly α photons are scattered away by intervening H I so that at the transition from atomic to molecular conditions in the disk atmosphere, the Ly α flux is roughly equal to flux of the (obliquely propagating) FUV continuum photons. A roughly similar ratio of Ly α to continuum photons is inferred observationally for the disk surface. In their analysis of the H₂ fluorescence emission from CTTS, Schindhelm et al. (2012) found that the flux of Ly α incident on the fluorescing H₂ layer (their F_{ab}) is 1.5–5 times larger than the continuum flux reaching the disk. Since some fraction of the stellar Ly α is absorbed or scattered away before reaching the fluorescing H₂, the Ly α flux incident on the H₂ is less than the stellar Ly α flux.

We therefore assume for our reference model that at the top of the atmosphere the ratio of the number flux of downward-propagating Ly α photons to the number flux of FUV continuum photons in the 1200–1700 Å band is $\eta = 3$, a value in the middle of the range reported by Schindhelm et al. (2012). We apply the methods described in AGN14 and assume a mean FUV continuum luminosity per 100 Å of $L_{\text{band}} = 1.1 \times 10^{30}$ erg s⁻¹. The FUV luminosities of CTTS can be an order of magnitude larger or smaller (Yang et al. 2012). The FUV continuum is absorbed by molecules and dust along the line of sight to the star. We improve on the treatment of the FUV continuum photoabsorption presented in AGN14 by treating a larger number of abundant molecules and atoms: H₂, CO, N₂, C, O₂, NH₃, HCN, CH₄, C₂H₂, and SO₂ in addition to H₂O and OH.

Ly α photons are also attenuated by dust and molecules, and we incorporate, in an approximate way,

scattering of Ly α by H I in the atmosphere. The scattering and absorption cross sections illustrate the relative roles of these processes for Ly α . The UV dust absorption cross section is 8×10^{-23} cm² per hydrogen, while the H₂O absorption cross section at Ly α is $\sigma_a(\text{H}_2\text{O}) \approx 10^{-17}$ cm² (van Dishoeck et al. 2006). For a typical water abundance of $x(\text{H}_2\text{O}) \approx 10^{-4}$,

$$\frac{\sigma_a(\text{dust})}{x(\text{H}_2\text{O})\sigma_a(\text{H}_2\text{O})} \approx 0.08. \quad (1)$$

Thus, water will typically dominate the UV opacity in the molecular layer.

To compare the roles of H₂O absorption and H I scattering for Ly α , we can consider a representative H I scattering cross-section. At ~ 80 Doppler widths (~ 300 km/s) from Ly α line center, where the Ly α line profile peaks in the spectrum of the CTTS TW Hya (Herczeg et al. 2004), the H I scattering cross section at that velocity is $\sigma_s(\text{H}) \approx 10^{-20}$ cm² (BB11). At the top of the molecular layer $x(\text{H})/x(\text{H}_2\text{O})$ ranges from 3×10^5 to 10, so that the ratio of H I scattering to H₂O absorption optical depths

$$\frac{x(\text{H})\sigma_s(\text{H})}{x(\text{H}_2\text{O})\sigma_a(\text{H}_2\text{O})} \approx 300 - 0.01. \quad (2)$$

The ratio in Eq. 2 is a sensitive function of depth into the atmosphere, because $x(\text{H})$ and $x(\text{H}_2\text{O})$ both depend strongly on vertical column. This comparison suggests that there may be regions where H I scattering can increase the path of Ly α photons through the absorbing medium, and can therefore increase the probability of absorption by H₂O.

To include Ly α absorption and scattering in a simple way, we can consider the scattering optical depth along a path length ℓ through a grid cell $\tau_s = n_s\sigma_s\ell = \ell/\ell_s$, where n_s and σ_s are the number density and cross section of scatterers, and ℓ_s is the scattering mean free path. To traverse a distance ℓ via a random walk, the Ly α photons will take approximately τ_s^2 steps. That is, scattered photons will travel a distance $\ell_{\text{eff}} = \tau_s^2\ell_s = \tau_s\ell$ through the absorbing medium. Because of the longer path length, the effective optical depth for absorption is

$$\tau_{\text{eff}} = n_a\sigma_a\ell_{\text{eff}} = (n_a\sigma_a\ell)\tau_s = \tau_a\tau_s \quad (3)$$

where n_a and σ_a are the number density and absorption cross section of absorbers (e.g., dust or molecules) and $\tau_a = n_a\sigma_a\ell$ is the usual absorption optical depth without scattering. As a result, for each grid step in the model, we calculate the scattering optical depth as

$$\tau_s = n(\text{H})\sigma_s(\text{H})\ell_z, \quad (4)$$

where ℓ_z is the vertical size of the grid cell, and approximate the increased probability of absorption in the presence of scattering by multiplying the normal absorption optical depth τ_a by a factor of τ_s when the scattering is large (i.e., $\tau_s > 1$). The increase in path length leads to increased Ly α absorption, which both attenuates the Ly α and increases the photochemical and photoelectric heating by Ly α . We also assume that fluorescent excitation of hot H₂ does not attenuate the Ly α , consistent with detailed modeling of UV fluorescent H₂ emission, which finds that only a small fraction of the incident Ly α

is processed into H₂ emission (2% for TW Hya; Herczeg et al. 2004). The photodissociation rate for species X is given as the sum of the dissociation rates from FUV continuum and Ly α photons,

$$G(X) = G_{\text{cont}} + G_{\text{Ly}\alpha}. \quad (5)$$

The continuum rate is

$$G_{\text{cont}} = \int_{\lambda_0}^{\lambda_f} F_{\text{cont}}(\lambda) \sigma(\lambda; X) d\lambda, \quad (6)$$

where $F_{\text{cont}}(\lambda)$ is the local FUV continuum photon number flux spectrum over wavelengths λ , which has been attenuated along the line of sight to the star and $\sigma(\lambda; X)$ is the photodissociation cross section spectrum for species X. Similarly, the photorate for dissociation by Ly α is

$$G_{\text{Ly}\alpha} = F_{\text{Ly}\alpha} \sigma(\text{Ly}\alpha; X), \quad (7)$$

where $F_{\text{Ly}\alpha}$ is the downward propagating Ly α number flux, and $\sigma(\text{Ly}\alpha; X)$ is the photodissociation cross section for species X at Ly α . References for the cross sections used here are given in Table A1.

The opacity of the 911 – 1108 Å band is dominated by the abundant species H₂, CO, N₂, and C. Most importantly, H₂, CO and N₂ absorb via lines and thus self- and mutually shield one another, as well as all other species. They therefore require detailed treatment of their opacity. Being the most abundant, H₂ is the most important absorber in the 911 – 1108 Å band. We use the H₂ shielding function given by Draine & Bertoldi (1996),

$$J(\text{H}_2) = \frac{0.965}{(1 + x/b_5)^\alpha} + \frac{0.035}{\sqrt{1+x}} e^{-8.5 \times 10^{-4} \sqrt{1+x}}, \quad (8)$$

where $x \equiv N(\text{H}_2)/5 \times 10^{14} \text{ cm}^{-2}$, $b_5 \equiv b/10^5 \text{ cm s}^{-1}$, and the Doppler broadening parameter is $b = 3 \text{ km s}^{-1}$. The original expression used $\alpha=2$ and applied to temperatures up to 300 K. Wolcott-Green et al. (2011) determined the shielding function in a 3D model and considered temperatures up to 10⁴ K. They found that using $\alpha = 1.1$ gives a better parameterization of the shielding at high temperatures, which we use here in calculating $J(\text{H}_2)$.

Tabulations of the shielding by CO as a function of $N(\text{H}_2)$ and $N(\text{CO})$ are provided by Visser et al. (2009) for a set of Doppler widths, excitations temperatures, and isotopologue ratios¹. We use the table for the conditions that most closely approximate the conditions in the molecular region of the disk, $b(\text{CO}) = 0.3 \text{ km s}^{-1}$, $T_{\text{ex}}(\text{CO}) = 100 \text{ K}$, and $^{12}\text{CO}/^{13}\text{CO}=69$, to lookup the CO shielding function $J(\text{CO})$. Similarly, Li et al. (2013) provide the shielding functions for N₂, and we use the shielding functions $J(\text{N}_2)$ tabulated for $b(\text{H}_2) = 3.0 \text{ km s}^{-1}$, $b(\text{N}_2) = 0.77 \text{ km s}^{-1}$, $T_{\text{ex}}(\text{N}_2) = T_{\text{ex}}(\text{H}_2) = 1000 \text{ K}$, and $N(\text{H}) = 10^{22} \text{ cm}^{-2}$.

For H₂, CO, and N₂, the first (continuum) term in the expression for $G(X)$ is decreased according to the shielding factors described above, as well as by all other continuum absorbers including dust grains. The absorption spectrum of C in the 911 – 1108 Å band is essentially continuum absorption, and for large N_{H} , the molecular

hydrogen shielding occurs in the far line wing, which covers a significant fraction of continuum. Therefore, H₂ may shield the ionization of atomic carbon, and so we estimate the attenuation of $G(\text{C})$ by a factor of $J(\text{H}_2)$, defined in Eq. 8.

2.2. X-rays with Compton Scattering

The theory for X-ray ionization presented in Ádámkóvics et al. (2011) and implemented in AGN14, uses a single temperature X-ray spectrum, and considers only the absorption of X-rays. Studies by Ercolano & Glassgold (2013), using a 3D radiative transfer and photoionization code with Compton scattering together with a more realistic two-temperature X-ray spectrum, show that ionization rates can be factors of several larger at low densities (and smaller at high densities) in the disk atmosphere than in our earlier calculations. Ercolano & Glassgold (2013) tabulate ionization rates calculated with depleted ISM elemental abundances for X-ray spectra that match the observations of the *Chandra* Orion Ultradeep Project (COUP). Since we consider the same disk density structure, we scale total ionization rates in Ádámkóvics et al. (2011) to match Ercolano & Glassgold (2013) at each altitude in the model, and we use this scaling to calculate the shell-specific ionization rates.

2.3. Thermal Processes: Photochemical heating by Ly α

Our thermal model includes the heating processes described in Glassgold et al. (2004) and AGN14: X-ray heating, accretion-related mechanical heating, thermal accommodation between gas and dust, grain photoelectric heating, photochemical heating by H₂O and OH, and H₂ formation heating. In addition we include photochemical heating for C, H₂, CO, H₂O, and OH following GN15, as well as O₂, which is described in the Appendix. We do not calculate the photochemical heating for NH₃, HCN, CH₄, C₂H₂, and SO₂ due to their small abundances. We include photochemical heating for H₂O and OH by Ly α photons, because these two molecules dominate the molecular opacity at Ly α . The photochemical heating from other species, which do not contribute significantly to the Ly α opacity, are ignored. Line cooling is essentially the same as in our earlier work and includes HI recombination lines, Ly α , H₂ vibrational and rotational transitions, CO rovibrational and pure rotational transitions, H₂O vibrational and rotational transitions, and O I forbidden and fine structure transitions. Above the atomic to molecular transition, Ly α cooling dominates and is supplemented at the transition by CO rovibrational, dust-gas and O I forbidden-line cooling.

In the prescription given in AGN14 for the chemical heating associated with the photodissociation of water and OH, roughly half of the photon energy in excess of the dissociation energy was converted to heating, primarily through collisions of the dissociation products. GN15 provide a more detailed description of the energetics of the dissociation products of these and other molecules and the thermal energy that could potentially be produced in their subsequent chemical reactions. The total heating due to the photodissociation of species X, $Q(X)$, is the sum of the direct heating component, $Q_{\text{dir}}(X)$, which arises from the translational energy of the disso-

¹ <http://home.strw.leidenuniv.nl/~ewine/photo/>

ciation products, and the chemical heating component, $Q_{\text{chem}}(X)$, which arises from the excitation of the products and their subsequent chemical reactions. The heating rate per photodissociation of each species is the sum of the heating by FUV continuum photons, $Q_{\text{cont}}(X)$, and by Ly α photons, $Q_{\text{Ly}\alpha}(X)$,

$$\Gamma_{\text{phchem}} = G_{\text{cont}} n Q_{\text{cont}} + G_{\text{Ly}\alpha} n Q_{\text{Ly}\alpha}, \quad (9)$$

where n is the volumetric number density of a particular species, having dropped the X from the notation.

Water and OH are the dominant sources of opacity for Ly α in the molecular layer as well as the dominant sources of photochemical heating. The photodissociation of H₂O by Ly α has three possible product channels (Harich et al. 2000), which were used in GN15 to calculate FUV continuum dissociation at wavelengths below 1450Å (their Band 2). In this band, GN15 obtained direct and chemical heating energies of $Q_{\text{dir}} = 0.24$ eV and $Q_{\text{chem}} = 0.86$ eV, respectively, for very high densities. We can apply the continuum results of GN15 that were based on experiments for Ly α photodissociation by simply raising the mean energy used in the GN15 treatment (9.67 eV), to the Ly α photon energy of 10.2 eV. For Ly α dissociation of H₂O, Q_{dir} becomes 0.8 eV and the total photochemical heating is $Q_{\text{Ly}\alpha}(\text{H}_2\text{O}) = Q_{\text{dir}} + Q_{\text{chem}} = 1.6$ eV. Similarly, we can recalculate the heating per OH dissociation in GN15 using the 10.2 eV Ly α photon instead of the mean FUV continuum photon energy. Taking into account the 4.4 eV dissociation energy of OH and the 2.0 eV excitation energy of the excited O(¹D₂) photoproduct, we have 3.8 eV of direct heating energy. The GN15 chemical heating energy is 2.6 eV, so that $Q_{\text{Ly}\alpha}(\text{OH}) = 6.4$ eV. The photochemical heating energies for FUV continuum and Ly α are listed in Table A1.

3. RESULTS

We calculate the vertical (altitude) structure of abundances x , and gas temperature T_g , at radial distances of 0.24, 0.48, and 0.95 AU, which are characteristic of the emitting regions inferred from H₂ line widths in CTTS (France et al. 2012, Table 4). Although many thermal processes are considered here, in general only a few play major roles in the disk atmosphere. For example, in the low density layer just above the atomic to molecular transition, accretion heating is balanced by Ly α cooling, but cooling by CO rovibrational emission and H₂ formation heating are also important. The dominant heating mechanisms are plotted as a function of the vertical column density of hydrogen from the top of the disk atmosphere N_{H} in Figure 1, along with the Ly α and FUV continuum fluxes, for a radial distance of $r = 0.24$ AU.

As shown in Figure 1, heating by H₂O, OH, and H₂ formation dominates other heating mechanisms at the top of molecular layer ($\log N_{\text{H}} = 21.5 - 21.7 \text{ cm}^{-2}$) and raises the temperature of the molecular gas above 1500 K. These heating processes can each exceed mechanical and photoelectric heating. The H₂ formation heating in the warm molecular layer is actually photochemical in origin, as discussed in GN15. Deeper into the molecular layer the FUV radiation (both continuum and Ly α) is shielded by both dust and molecules and neither mechanism has an important role in heating the atmosphere.

Figure 2 shows the vertical profiles of key molecular abundances and temperatures plotted for the reference

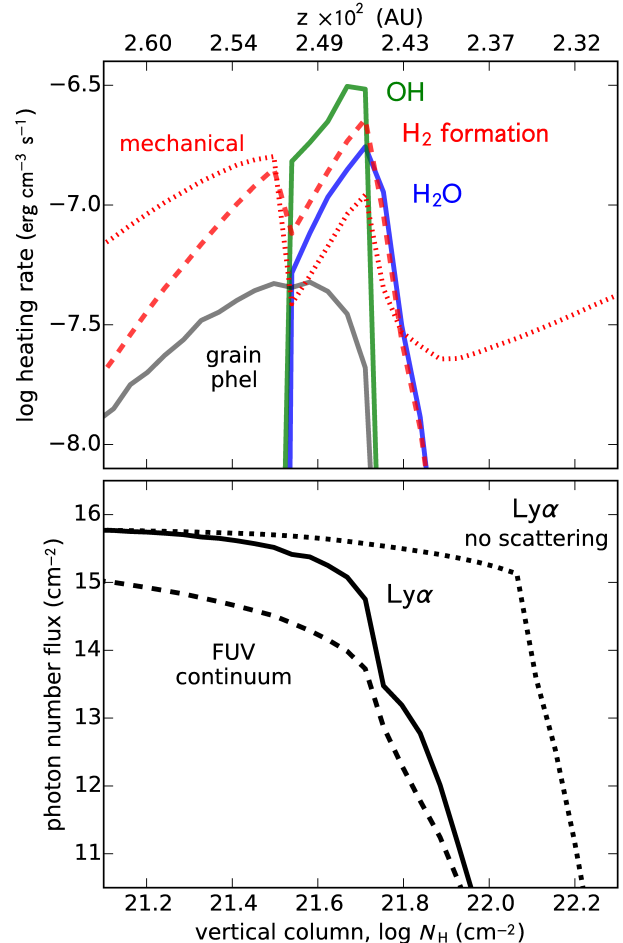


Figure 1. Vertical profiles of the thermal rates at $r = 0.24$ AU for the dominant heating mechanisms are shown in color in the top panel. The FUV heating is dominated by the photodissociation of molecules, primarily H₂O and OH by Ly α (blue and green curves, respectively), along with the closely related heating due to H₂ formation on grains (red dashed curve). Photoelectric heating on dust (grey curve) and mechanical heating (red dotted curve) are important in the atomic region at vertical columns less than $\log N_{\text{H}} \approx 21$. Vertical profiles of the photon number fluxes (bottom panel) for the FUV continuum (black dashed curve), Ly α in the absence of scattering (black dotted curve), and Ly α including the additional opacity due to scattering described in Equation 3 (black solid curve). A physical distance scale for the altitude above the midplane is given on the top axis.

model (solid curves), and for comparison we also show the results for a model without Ly α (dotted curves), which are essentially the same as our earlier reference model (i.e., the top left panel of Figure 5 in AGN14). In the absence of Ly α , there is a steep transition to peak $x(\text{H}_2)$ and peak $x(\text{H}_2\text{O})$ near $\log N_{\text{H}} = 21.4 \text{ cm}^{-2}$ and after the transition there is a steady decline in gas temperature and $x(\text{OH})$ with increasing N_{H} . Thus as in earlier models, the disk atmosphere is characterized by a hot (~ 5000 K) atomic layer that overlies a cooler (~ 1000 K) molecular layer. The region between these two layers is where the role of FUV radiation and photochemistry is most important, with the strength of the radiation field determining whether there is a sharp or a gradual transition from atomic to molecular conditions (AGN14).

As illustrated by our reference model with Ly α (solid

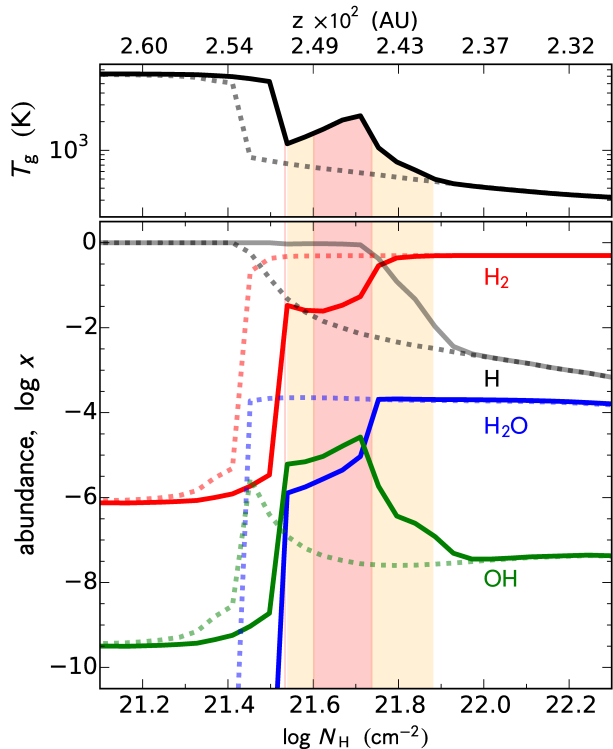


Figure 2. Vertical profiles of molecular abundances and gas temperature in the reference model of the disk atmosphere at $r = 0.24$ AU (solid curves). The red shaded region highlights the location of gas that is sufficiently hot for UV fluorescence from H_2 , where T_g is in the range 1500 – 2500 K. The orange shaded region is where T_g is in the range 500 – 1500 K. Dotted curves are from a model that has no $\text{Ly}\alpha$. A physical distance scale for the altitude above the midplane is given on the top axis.

curves in Figure 2), $\text{Ly}\alpha$ radiation is important for both heating the gas and photodissociating molecules near the transition. With $\text{Ly}\alpha$ included, the transition occurs deeper than with FUV continuum radiation alone, and e.g., the abundance of molecules such as H_2 and H_2O are reduced near $\log N_{\text{H}} \approx 21.6 \text{ cm}^{-2}$. This is similar to the effect of increasing the FUV continuum luminosity when $\text{Ly}\alpha$ is absent (Figure 4 in AGN14). Since the vertical optical depth of the atmosphere is roughly an order of magnitude less than the line of sight optical depth, the downward propagating $\text{Ly}\alpha$ penetrates deeper into regions of higher density than the FUV continuum, which travels along an oblique line-of-sight from the star. In contrast to our models without $\text{Ly}\alpha$, the gas temperature T_g in our reference model increases with vertical column N_{H} after the transition, from $\log N_{\text{H}} = 21.5$ through 21.7 cm^{-2} as a result of photochemical heating by $\text{Ly}\alpha$. The red shaded region in Figure 2 highlights the layer of hot molecular gas, where T_g is 1500 – 2500 K. The total column of H_2 in this region is $4.9 \times 10^{19} \text{ cm}^{-2}$. In the absence of $\text{Ly}\alpha$ the gas temperature is much lower, and there is no region of the atmosphere where H_2 is both abundant and hot.

The depth to which the FUV penetrates determines where hot molecular gas is present. As a result, the total column of hot molecular gas is sensitive to the magnitude of the FUV. Since we assume that the downward $\text{Ly}\alpha$ number flux is a factor of $\eta = 3$ larger than the

FUV continuum number flux at the top of the atmosphere (see Section 2.1), an order of magnitude increase in the FUV continuum leads to an order of magnitude more $\text{Ly}\alpha$ and produces a factor of ~ 4 times more hot H_2 (Table 2) at 0.24 AU. Increasing $\text{Ly}\alpha$ also leads to higher temperatures at larger radii. While there is no significant column of hot H_2 in the reference model at $r = 0.48$ AU (with $L_{\text{FUV}} = 10^{31} \text{ erg s}^{-1}$), and order of magnitude increase in $F_{\text{Ly}\alpha}$ leads to significant columns ($> 10^{19} \text{ cm}^{-2}$) of hot gas out to 0.48 AU in the disk.

On the other hand, a reduction in the FUV radiation has an even more dramatic effect on the column of hot molecular gas. We varied the radiation by decreasing both the FUV continuum and $\text{Ly}\alpha$; we also removed $\text{Ly}\alpha$ entirely by setting $F_{\text{Ly}\alpha} = 0$. In either case, the column of hot H_2 drops significantly. In models with either $L_{\text{FUV}} = 10^{30} \text{ erg s}^{-1}$ or no $\text{Ly}\alpha$, the maximum temperature in the irradiated molecular layer is below 1500 K, and the column of hot H_2 is four decades smaller (Table 2). In these cases, the only region of the atmosphere where $T_g > 1500 \text{ K}$ is in the hot atomic layer, where $x(\text{H}_2) \lesssim 10^{-5}$. As a result of the small abundance of H_2 , the total column of hot H_2 in the atomic layer is only $\sim 10^{15} \text{ cm}^{-2}$. This is the characteristic minimum value in Table 2 that indicates the lack of a hot molecular region. While both FUV continuum and $\text{Ly}\alpha$ are important for heating, the absence of a hot molecular region when $\text{Ly}\alpha$ is removed – while the FUV continuum is maintained – suggests that $\text{Ly}\alpha$ plays a more important role than the continuum in producing hot molecular gas. Again, this is because the downward propagating $\text{Ly}\alpha$ photons penetrate deeper than the continuum.

The depth to which $\text{Ly}\alpha$ photons penetrate depends on scattering in the hot molecular region. To illustrate the role of scattering we considered a case of pure absorption, i.e., only dust and molecular absorption and no H I scattering, which leads to the deepest penetration of radiation (black dotted curve in the bottom panel of Figure 1) and nearly an order of magnitude increase in the columns of hot H_2 than when scattering is included (Table 2). The column of hot H_2 is also sensitive (obviously) to $\eta = F_{\text{Ly}\alpha}/F_{\text{cont}}$ at the top of the atmosphere (Figure 3). When $\text{Ly}\alpha$ is reduced by a factor of 3 relative to our reference model (setting $\eta = 1$) the gas is heated to barely above 1500 K. An increased value of $\eta = 5$ results in a higher peak temperature for the hot H_2 and deeper penetration of the radiation into the disk.

Two other parameters in the model that are generally important for heating are the accretion-related mechanical heating parameter α_{h} , defined in Glassgold et al. (2004), and the dust grain size parameter, a_{g} . Mechanical heating is the dominant heating term deep in the disk and in the hot atomic region, while dust-gas thermalization is the dominant cooling mechanism at large column densities. Table 2, which shows the hot H_2 columns for cases with reduced α_{h} , larger a_{g} , or a combination of the two, illustrates the sensitivity of our results to these parameters. Effectively eliminating mechanical heating by reducing $\alpha_{\text{h}} = 0.01$ does not reduce the column of hot H_2 (Table 2). This is because mechanical heating is subdominant to photochemical heating and H_2 formation heating in the region of hot H_2 (Figure 1). Indeed, reducing α_{h} decreases the heating of the atomic layer, so

Table 2
Hot H₂ Column Densities^a and Model Parameters

Calculation	Radius (AU)			Parameters ^b		
	0.24	0.48	0.95	α_h	a_g	L_{FUV}
Reference ^c α_h, a_g	3.6(15)	3.1(15)	3.8(15)	0.50	0.71	1(30)
	4.9(19)	3.2(15)	3.6(15)	0.50	0.71	1(31)
	2.0(20)	3.6(19)	4.5(15)	0.50	0.71	1(32)
Reduced α_h	6.4(15)	1.1(17)	1.2(17)	0.01	0.71	1(30)
	7.3(19)	6.0(15)	8.0(15)	0.01	0.71	1(31)
	1.9(20)	5.0(19)	3.5(15)	0.01	0.71	1(32)
Larger a_g	1.2(15)	2.2(15)	1.6(15)	0.50	7.07	1(30)
	1.4(15)	1.6(15)	2.0(15)	0.50	7.07	1(31)
	3.4(20)	9.9(18)	2.4(15)	0.50	7.07	1(32)
Reduced α_h , larger a_g	1.1(15)	2.5(15)	1.9(16)	0.01	7.07	1(30)
	3.9(19)	5.8(19)	2.5(16)	0.01	7.07	1(31)
	9.5(19)	3.8(19)	3.3(19)	0.01	7.07	1(32)
No Ly α	3.7(15)	2.9(15)	3.6(15)	0.50	0.71	1(31)
$\eta = 1$	2.8(19)	3.1(15)	3.4(15)	0.50	0.71	1(31)
$\eta = 3^c$	4.9(19)	3.2(15)	3.6(15)	0.50	0.71	1(31)
$\eta = 5$	5.7(19)	2.4(19)	3.7(15)	0.50	0.71	1(31)
No Ly α scattering	2.9(20)	1.7(20)	3.6(15)	0.50	0.71	1(31)

^a Column densities for gas temperatures $T > 1500$ K in units of cm^{-2} , with values above 10^{18}cm^{-2} , which indicate a hot H₂ region, highlighted in bold.

^b Parameter units: α_h is the dimensionless accretion-related mechanical heating parameter; a_g is the grain size parameter in μm ; and L_{FUV} is the FUV continuum luminosity in erg s^{-1} .

^c The reference model that is plotted for $r = 0.24$ AU in the Figures.

that the transition from atomic to molecular conditions occurs at a higher altitude in the disk atmosphere (Figure 4). Models with smaller α_h therefore have columns of hot H₂ that are somewhat larger than the reference model, by a factor of $\sim 50\%$ (Table 2).

The dust in the atmosphere plays competing roles as an important opacity source for the FUV, as the catalyst for H₂ formation and therefore H₂ formation heating, and as an important coolant via thermal accommodation in regions of high density. Increasing the grain size parameter, a_g , reduces the surface area and opacity of the dust, reduces H₂ formation heating, and allows the FUV to penetrate deeper into the disk. With larger dust grains, the transition from atomic to molecular conditions occurs at a lower altitude in the disk atmosphere, where the densities are higher (AGN14). For the reference FUV continuum luminosity ($L_{\text{FUV}} = 10^{30} \text{erg s}^{-1}$) and large grains ($a_g = 7.07 \mu\text{m}$), the transition is from hot atomic conditions to cool, fully molecular conditions, and there is no region of hot H₂. However, models with increased radiation as well as with large grains produce the largest columns of hot H₂ (Table 2), as the irradiated molecular layer occurs deeper into the disk (Figure 4). The details of the dominant thermal and chemical changes due to variations in α_h , a_g , and L_{FUV} are complex. However, as these parameter variations illustrate, hot H₂ columns $\sim 10^{19} \text{cm}^{-2}$ are a common outcome for a range of a_g and α_h values.

4. DISCUSSION

We find that including Ly α in our earlier model of a disk atmosphere irradiated by FUV continuum and X-rays (AGN14) produces a new component of the inner disk atmosphere: a region of hot molecular gas (1500 – 2500 K; Figure 2). The reason for the difference is related to the distinctive radiative transfer and propagation path of the Ly α photons more than to their lu-

minosity. Although the Ly α component is much more luminous than the FUV continuum in the present case, the total FUV luminosity (continuum + Ly α) is similar to that assumed in AGN14. More significantly, the Ly α fraction of the FUV luminosity propagates more directly downward through the disk compared to the FUV the continuum, which propagates along an oblique line-of-sight into the disk. As shown in Table 2, a hot molecular component occurs under a wide range of conditions. The column density of hot H₂ is insensitive to the value of the mechanical heating parameter α_h . Column densities of hot H₂ $> 10^{19} \text{cm}^{-2}$ are obtained for a range of FUV luminosities, (i.e., FUV continuum luminosities 0.0025 – 0.025 L_{\odot}). Large column densities are also found when both the grain size parameter and mechanical heating are reduced.

The FUV continuum luminosities we considered span the middle to upper range among TTS (Yang et al. 2012) and are consistent with the properties of sources with well-studied hot H₂ (France et al. 2012; Schindhelm et al. 2012). The properties of the hot H₂ found in the models (temperature, column density, radial distance) are similar to those inferred for the UV fluorescent molecular hydrogen emission from T Tauri stars. For example, in their study of H₂ emission from TW Hya, Herczeg et al. (2004) inferred an excitation temperature of $T_{\text{ex}} = 2500 (+700/-500)$ K, an H₂ column density of $\log N(\text{H}_2) = 18.5(+1.2/-0.8) \text{cm}^{-2}$, and constrained the source of the emission to radial distances within 2 AU. Schindhelm et al. (2012) reported similar conditions for the UV fluorescent H₂ emission from a larger sample of T Tauri stars ($T(\text{H}_2) = 2500 \pm 1000$ K, $\log N(\text{H}_2) = 19 \pm 1 \text{cm}^{-2}$). The H₂ line profiles reported in France et al. (2012) for single, normal (non-transition) TTS suggest that the emission arises typically from radii $\sim 0.1-1$ AU.

In the above studies, the T Tauri stars that show flu-

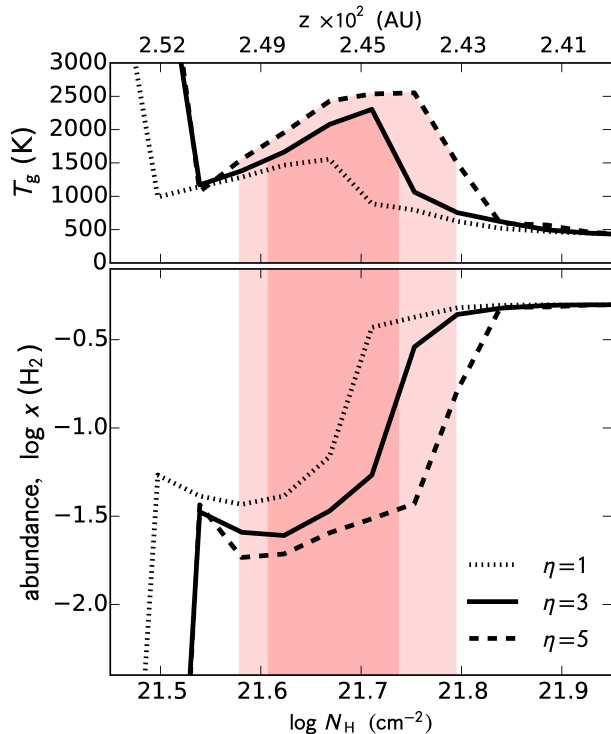


Figure 3. Vertical profiles of gas temperatures and H₂ abundances for different Ly α radiation fluxes at $r = 0.24$ AU, highlighting the role of Ly α in determining the extent of the region of hot H₂. The reference model has $\eta = 3$ (solid curves), and the region of hot H₂ is highlighted in the darker shaded region. Also shown are models with $\eta = 1$ (dotted), which barely exceeds 1500 K in the molecular layer, as well as models with $\eta = 5$ (dashed), where both the maximum T_g and the depth of the hot H₂ region are increased relative to the reference model (lighter shaded region). A physical distance scale for the altitude above the midplane is given on the top axis.

orescent H₂ emission include sources that have experienced significant grain settling relative to ISM values. The Taurus sources in Schindhelm et al. (2012) span a range of 10 μ m silicate emission equivalent widths (0.22 – 1.0) and MIR colors ($n_{13-25} = -0.4$ to 0.2; Furlan et al. 2006), which are consistent with grain area reduction by a factor ~ 100 . The best fits in the Herczeg et al. (2004) modeling of the fluorescent H₂ emission from TW Hya have the H₂ mixed with little dust compared to an ISM grain abundance (they assumed no dust). These conditions are similar to the reduced grain area adopted in our models.

The hot H₂ occurs in a region that is primarily atomic, $x(\text{H}_2)/x(\text{H}) < 0.1$, and mixed with a high abundance of water, $x(\text{H}_2\text{O}) \sim 10^{-5}$. Thus, both scattering and photochemical heating are important in this region of the atmosphere. Interestingly, Ly α reconstruction studies typically assume that the UV fluorescent H₂ occurs in a region with little HI (Herczeg et al.; Schindhelm et al.). Our results suggest that HI scattering could play a larger role, potentially increasing the likelihood of Ly α excitation of hot H₂, similar to the increased probability of Ly α absorption by dust or water when HI scattering occurs.

As noted in France et al. (2012), the UV fluorescent H₂ emission profiles indicate that the emission arises

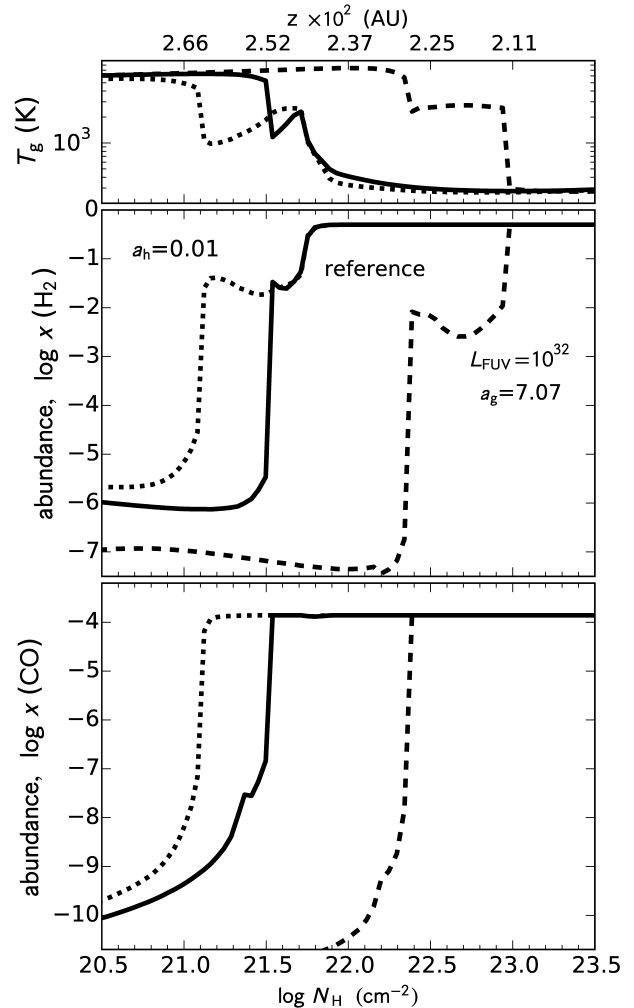


Figure 4. Vertical profiles of T_g , $x(\text{H}_2)$, and $x(\text{CO})$ with different values for α_h , a_g , and L_{FUV} at $r = 0.24$ AU. Profiles from a model with reduced mechanical heating (dotted curves) have a transition higher in the atmosphere, while models with larger grains and increased radiation (dashed curves) transition to molecular conditions deeper into the atmosphere. A physical distance scale for the altitude above the midplane is given on the top axis.

from similar disk radii as the CO rovibrational emission from disks (Salyk et al. 2011, e.g.,). Our model also produces an enhanced column density of hot ($T > 900$ K) CO, with columns in the $10^{17} - 10^{18} \text{ cm}^{-2}$ range, generally from within 1 AU. For models with large grain sizes ($a_g = 7.07 \mu\text{m}$) in the upper range of FUV luminosity ($L_{\text{FUV}} = 0.025 L_{\odot}$), a significant fraction of radiation penetrates deep into the disk and we see columns of up to $2 \times 10^{18} - 8 \times 10^{18} \text{ cm}^{-2}$ of hot CO within 0.5 AU (Figure 4). These values compare favorably to the CO rovibrational emission properties of T Tauri disks (e.g., Najita et al. 2003). Salyk et al. (2011) reported line-of-sight CO emission columns of $10^{18} - 10^{19} \text{ cm}^{-2}$ and excitation temperatures of 900–1600 K for a sample of Taurus disks; the small CO emitting areas and the width of the emission lines are consistent with much of the emission arising from < 0.4 AU. Thus, the enhanced hot H₂ and CO that we find in the hot atomic and warm irradiated layers of our model may help to explain the UV fluores-

cent H₂ and CO rovibrational emission that is commonly observed from T Tauri disks.

The study by Nomura et al. (2007) provides an interesting counterpoint to the current study. In their pioneering work on the excitation of H₂ in disks, Nomura et al. (2007) illustrated how protoplanetary disks that are irradiated by stellar UV and X-rays could produce detectable H₂ emission at UV and IR wavelengths. There are many differences between the two models, e.g., the chemical model used here is more detailed and molecular shielding is included, but hydrostatic equilibrium is not enforced and the H₂ level populations are not calculated. However, one of the most interesting differences between the two models is the way in which the stellar UV heats the gas. In Nomura et al. (2007), the gas is heated by UV photons through grain photoelectric heating. As grains settle out of the disk atmosphere, grain photoelectric heating is reduced, the temperature of the gaseous atmosphere drops, and the H₂ emission declines in strength. These results led Nomura et al. to conclude that H₂ emission will be strongest from disks with an abundant small grain population, i.e., disks that have experienced little grain growth and settling. In contrast, H₂ emission is detected commonly from TTS, the majority of which have experienced significant grain settling.

In our model, UV photons heat the gas primarily through photodissociation of OH and H₂O. While photoelectric heating is included in our calculation, it plays a limited role because of the reduced abundance of small grains in the atmosphere. In this way, heating by UV remains strong even as grains settle out of the atmosphere. Indeed, as the grains settle, the FUV radiation penetrates deeper, and larger columns of hot H₂ and CO are produced.

Our models complement the disk model of Du & Bergin (2014) in both the methods employed and the astrophysical issues that are addressed. In Du & Bergin (2014), Ly α propagation is treated in a much more sophisticated way and photochemical heating is included in a simplified way compared to the methods used here. As in AGN14, Du & Bergin (2014) focussed on the distribution of warm water and primarily on the region > 1 AU in contrast to the smaller radii considered here. While Du & Bergin (2014) did not address in their work the origin of fluorescent H₂, the methods used in their work could be used to investigate this question in

greater detail.

In summary, we find that the Ly α component of the FUV radiation field of young stars has a significant impact on the thermal structure of disk atmospheres. Ly α photons scattered by H I at the top of the disk atmosphere deposit their energy deeper in the disk atmosphere than radially propagating FUV continuum photons. In addition, scattering by H I throughout the upper disk atmosphere can cause much of the Ly α energy to be deposited over a restricted range in column density, which leads to a surface layer of hot H₂. The temperature in the layer is high enough (~ 2000 K) to thermally excite the H₂ to vibrational levels from which they can be fluoresced by Ly α to produce the UV fluorescent H₂ emission that is characteristic of accreting young stars. Ly α irradiation also leads to a layer of warm CO (> 900 K) in the inner disk atmosphere that has a column density similar to that inferred for $4.7 \mu\text{m}$ rovibrational CO emission from young stars. The high H₂ and CO temperatures are primarily the result of photochemical heating (by H₂O, OH and H₂ formation), a process that offers an efficient way to tap energy of the stellar UV field when grains have settled out of disk atmospheres and photoelectric heating is diminished.

We have investigated the impact of Ly α heating on a particular disk atmosphere model. Given the significant impact of Ly α irradiation on the thermal structure of the disk atmosphere, it is important to examine its role relative to other processes over a range of disk radii. More generally, we have investigated the impact of Ly α heating in the context of one particular disk atmosphere model. Further studies of the impact of Ly α heating under a wider range of disk conditions would be useful to understand the general nature of this process.

ACKNOWLEDGMENTS

We acknowledge helpful conversations with Greg Herzeg and Kevin France, and support from the following NASA grants: NNX15AE24G (Exoplanets Research Program), NNG06GF88G (Origins), 1367693 (*Herschel* DIGIT), and Agreement No. NNX15AD94G for the program ‘‘Earths in Other Solar Systems’’. This work was performed in part at the Aspen Center for Physics, which is supported by National Science Foundation grant PHY-1066293.

APPENDIX

A. FUV PHOTOCHEMICAL HEATING OF O₂

The photochemical heating discussed in Sec. 2 is based on GN15. However, the examples treated there do not include O₂ which can play a significant role in the FUV heating of the molecular layer. The photochemical heating defined in Eq. 1 is composed of a direct and a chemical part,

$$Q_{\text{phchem}} = Q_{\text{dir}} + Q_{\text{chem}}, \quad (\text{A1})$$

where Q_{dir} comes from the kinetic energy of the dissociation fragments (two O atoms in this case), and Q_{chem} from their chemical energies. As emphasized by GN15, photochemical heating is dependent on the density because some of it arises from excitation of the products and only leads to heating if the density is high enough for collisional de-excitation of the excited levels to occur. In the present application to the molecular layer, the densities are high enough ($> 10^{10} \text{ cm}^{-3}$) that it is a good approximation to assume that essentially all excitation goes into heating.

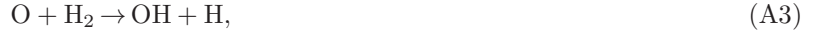
The UV absorption cross section of O₂ is well known. It is dominated by the Schumann-Runge continuum from 1300–1800 Å, well measured by Yoshino et al. (2005). Over much of this band, one of the atoms is produced in the ¹D₂ level (Lee & Nee 2000, 2001). Following GN15, we assume that all of the excitation energy, $E(^1\text{D}_2) = 1.98 \text{ eV}$, is

available for heating. Below 1400 Å, the branching ratio b for the 1D_2 level is less than one, but this only reduces the mean heating from its collisional de-excitation by $\sim 10\%$. The 1S_0 level at 4.19 eV is also produced below 1100 Å, but it quickly decays to the 1D_2 level. In any case, these wavelengths are heavily blocked by H_2 and CO self-shielding, and we ignore O_2 heating in the 900-1100 Å band.

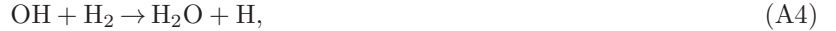
The direct heating has been obtained by calculating the the mean value of the quantity,

$$\Delta E_{\text{dir}} = h\nu - D(O_2) - bE(^1D_2), \quad (\text{A2})$$

in each of ten 100 Å bands from 1100-2400 Å; the dissociation energy of O_2 has been set to $D(O_2) = 5.12$ eV, and the mean value of b is $\bar{b} = 0.90$. The result is $Q_{\text{dir}} = 1.6$ eV. The chemical energy is obtained from the reactions, initiated by each O atom,



and,



which are equivalent to,



with a net energy yield of 0.57 eV. Thus the net chemical energy is $Q_{\text{chem}} = 2(0.57 + \bar{b}1.98)$ eV or 4.7 eV, and the total photochemical heating is $Q_{\text{phchem}}(O_2) = 6.3$ eV. For the same conditions, the photochemical heating of H_2O and OH are 2.1 eV and 5.5 eV, respectively. The heating rates in Figure 1 reflect these values together with the abundances of the oxygen molecules.

REFERENCES

- Ádámkóvics, M., Glassgold, A. E., & Meijerink, R. 2011, *ApJ*, 736, 143
 Ádámkóvics, M., Glassgold, A. E., & Najita, J. R. 2014, *ApJ*, 786, 135 (AGN14)
 Agúndez, M., Cernicharo, J., & Goicoechea, J. R. 2008, *A&A*, 483, 831
 Aikawa, Y., & Herbst, E. 1999, *A&A*, 351, 233
 Akimkin, V., Zhukovska, S., Wiebe, D., et al. 2013, *ApJ*, 766, 8
 Ardila, D. R., Basri, G., Walter, F. M., Valenti, J. A., & Johns-Krull, C. M. 2002, *ApJ*, 567, 1013
 Bergin, E., Calvet, N., D'Alessio, P., & Herczeg, G. J. 2003, *ApJ*, 591, L159
 Bethell, T., & Bergin, E. 2009, *Science*, 326, 1675
 Bethell, T. J., & Bergin, E. A. 2011, *ApJ*, 739, 78
 Cleaves, L. I., Bergin, E. A., Bethell, T. J., et al. 2011, *ApJ*, 743, L2
 D'Alessio, P., Calvet, N., Hartmann, L., Lizano, S., & Cantó, J. 1999, *ApJ*, 527, 893
 Draine, B. T., & Bertoldi, F. 1996, *ApJ*, 468, 269
 Du, F., & Bergin, E. A. 2014, *ApJ*, 792, 2
 Ercolano, B., Clarke, C. J., & Drake, J. J. 2009, *ApJ*, 699, 1639
 Ercolano, B., & Glassgold, A. E. 2013, *MNRAS*, 436, 3446
 Fogel, J. K. J., Bethell, T. J., Bergin, E. A., Calvet, N., & Semenov, D. 2011, *ApJ*, 726, 29
 France, K., Schindhelm, E., Herczeg, G. J., et al. 2012, *ApJ*, 756, 171
 Furlan, E., Hartmann, L., Calvet, N., et al. 2006, *ApJS*, 165, 568
 Glassgold, A. E., Meijerink, R., & Najita, J. R. 2009, *ApJ*, 701, 142
 Glassgold, A. E., Najita, J., & Igea, J. 2004, *ApJ*, 615, 972 (GNI04)
 Glassgold, A. E., & Najita, J. R. 2015, *ApJ*, 810, 125
 Gorti, U., & Hollenbach, D. 2004, *ApJ*, 613, 424
 —. 2008, *ApJ*, 683, 287
 Gorti, U., Hollenbach, D., Najita, J., & Pascucci, I. 2011, *ApJ*, 735, 90
 Harich, S. A., Hwang, D. W. H., Yang, X., et al. 2000, *JChPh*, 113, 10073
 Heinzeller, D., Nomura, H., Walsh, C., & Millar, T. J. 2011, *ApJ*, 731, 115
 Herczeg, G. J., Linsky, J. L., Valenti, J. A., Johns-Krull, C. M., & Wood, B. E. 2002, *ApJ*, 572, 310
 Herczeg, G. J., Wood, B. E., Linsky, J. L., Valenti, J. A., & Johns-Krull, C. M. 2004, *ApJ*, 607, 369
 Jonkheid, B., Faas, F. G. A., van Zadelhoff, G.-J., & van Dishoeck, E. F. 2004, *A&A*, 428, 511
 Kamp, I., & Dullemond, C. P. 2004, *ApJ*, 615, 991
 Lee, L. C., & Suto, M. 1986, *CP*, 110, 161
 Lee, P. C., & Nee, J. B. 2000, *JChPh*, 112, 1763
 —. 2001, *JChPh*, 114, 792
 Li, X., Heays, A. N., Visser, R., et al. 2013, *A&A*, 555, A14
 Markwick, A. J., Ilgner, M., Millar, T. J., & Henning, T. 2002, *A&A*, 385, 632
 McGuire, E. J. 1968, *PhRv*, 175, 20
 Mota, R., Parafita, R., Giuliani, A., et al. 2005, *CPL*, 416, 152
 Najita, J., Carr, J. S., & Mathieu, R. D. 2003, *ApJ*, 589, 931
 Najita, J. R., Ádámkóvics, M., & Glassgold, A. E. 2011, *ApJ*, 743, 147
 Nomura, H., Aikawa, Y., Tsujimoto, M., Nakagawa, Y., & Millar, T. J. 2007, *ApJ*, 661, 334
 Parkinson, W. H., & Yoshino, K. 2003, *CP*, 294, 31
 Salyk, C., Pontoppidan, K. M., Blake, G. A., Najita, J. R., & Carr, J. S. 2011, *ApJ*, 731, 130
 Schindhelm, E., France, K., Herczeg, G. J., et al. 2012, *ApJ*, 756, L23
 van Dishoeck, E. F., & Dalgarno, A. 1984, *ApJ*, 277, 576
 van Dishoeck, E. F., Jonkheid, B., & van Hemert, M. C. 2006, *FaDi*, 133, 231
 van Zadelhoff, G.-J., Aikawa, Y., Hogerheijde, M. R., & van Dishoeck, E. F. 2003, *A&A*, 397, 789
 Visser, R., van Dishoeck, E. F., & Black, J. H. 2009, *A&A*, 503, 323

Table A1
Photochemical heating energies and cross sections^a

X ^b	Q_{cont}	$Q_{\text{Ly}\alpha}$	$\sigma_X(\text{Ly}\alpha)^c$	Refs. ^d
H ₂ O	2.1	1.6	12	1
OH	5.5	6.4	1.8	2
O ₂	6.3	...	0.01	3
H ₂	12.5	4
CO	8.7	5
C	8.0	6
N ₂	7

^a Units for photochemical heating energies are eV per photodissociation and cross sections are in 10^{-18} cm².

^b The species that contribute to FUV continuum photochemical heating have numerical values in second column, Q_{FUV} , and those considered for Ly α photochemical heating have values listed in the third column for $Q_{\text{Ly}\alpha}$.

^c Ly α cross sections from van Dishoeck et al. (2006). The molecules that cannot be dissociated from their ground state by Ly α do not have cross sections listed.

^d References for FUV continuum cross sections: (1) Lee & Suto (1986); Parkinson & Yoshino (2003); Mota et al. (2005); (2) van Dishoeck & Dalgarno (1984); (3) Yoshino et al. (1992, 2005); References for line shielding: (4) Draine & Bertoldi (1996); (5) Visser et al. (2009); (6) McGuire (1968); (7) Li et al. (2013).

Walsh, C., Nomura, H., Millar, T. J., & Aikawa, Y. 2012, [ApJ](#), **747**, 114

Willacy, K., & Langer, W. D. 2000, [ApJ](#), **544**, 903

Woitke, P., Kamp, I., & Thi, W.-F. 2009, [A&A](#), **501**, 383

Wolcott-Green, J., Haiman, Z., & Bryan, G. L. 2011, [MNRAS](#), **418**, 838

Woods, P. M., & Willacy, K. 2009, [ApJ](#), **693**, 1360

Yang, H., Herczeg, G. J., Linsky, J. L., et al. 2012, [ApJ](#), **744**, 121

Yoshino, K., Esmond, J. R., Cheung, A. S.-C., Freeman, D. E., & Parkinson, W. H. 1992, [P&SS](#), **40**, 185

Yoshino, K., Parkinson, W. H., Ito, K., & Matsui, T. 2005, [JMoSp](#), **229**, 238